1

Advanced Applications of NEXAFS Spectroscopy for Functionalized Surfaces

Alexei Nefedov and Christof Wöll

Institute of Functional Interfaces, Karlsruhe Institute of Technology,
Hermann-von-Helmholtz-Platz 1, 76344 Eggenstein-Leopoldshafen, Germany
alexei.nefedov@kit.edu

Abstract. Spectroscopic techniques based on the use of synchrotron radiation have significantly contributed to a better understanding of macroscopic as well as of microscopic properties of materials. One of them is near edge X-ray absorption fine structure (NEXAFS) spectroscopy, a source of valuable information on the electronic structure and orientation of molecular adsorbates on metal surfaces. NEXAFS spectroscopy has had its largest impact in connection with an electron-based detection of the photon absorption, which turns this technique in a highly surface sensitive method. The technique has been developed over the past 30 years and presently is routinely used to study the adsorption of organic molecules on a large variety of different substrates, including metals, oxides and polymers. In the last decades, in addition to above-mentioned systems, the spectroscopic characterization of nanostructures has become an important topic. The present contribution describes the basics of NEXAFS spectroscopy and demonstrates the potential of the method by discussing several case studies.

1.1 Introduction

Reliable and precise knowledge about the geometric and electronic properties are of utmost importance for a fundamental understanding of the macroscopic and microscopic behavior of materials. For functionalized interfaces this rather general statement is even more true since the enormous importance of such properties for the general behavior of nano-, macro- and micro-scaled systems is paralleled by a huge experimental challenge to gather this information. These problems are caused by the fairly small amount of material which governs the properties of an interface. A reliable characterization of interface properties requires the utilization of highly surface sensitive methods. X-ray diffraction methods, the standard tool to obtain information on geometric structure and in particular on the orientation of molecules in the bulk, cannot be applied to ultrathin layers of molecules of surfaces in a direct fashion, since

sensitivity problems, a fairly small threshold for radiation damage represent major experimental challenges in this area.

Among the different tools and techniques developed for the exploration of electronic and structural properties of interfaces synchrotron based methods have played a prominent role. Synchrotrons have first been built in the 1940s, mainly for applications in nuclear physics, and synchrotron radiation (SR) was first used in the "parasitic" mode of operation. Only when – some 50 years ago – second generation machines devoted to the use of SR for the characterization of materials were built, the method started to generate a larger impact on the understanding of physical and chemical properties of surfaces. Over the last three decades, second and more recently also third generation synchrotrons have contributed significantly to a better understanding of materials on the molecular and macroscopic scale. The large impact of SR in the area of surface science mainly results from information obtained via photoelectron spectroscopy. Due to the fairly short exit depth of photoelectrons excited in a solid substrate by absorption of photons, all variants of photoelectron spectroscopy based on electron detection are highly surface sensitive.

With regard to the chemical characterization of materials X-ray photoelectron spectroscopy (XPS) carried out with laboratory sources is the method which has had the largest impact in the field; in fact, laboratory X-ray sources are used in virtually every laboratory focusing on surface science, including the area of industrial research. Being able to set the incident energy of the photons to arbitrary values – and not being limited to the rather selected values of photon energies available from standard X-ray tubes – certainly already generates a huge potential; e.g, just setting the incident energy 30–50 eV higher than the core level binding energy increases the cross section by more than an order of magnitude.

In this chapter, however, we focus on a different variant of synchrotron-based photoelectron spectroscopy, one where the incident energy of the photons is continuously varied over a certain energy range. This method has the obvious disadvantage that it cannot be used in a connection with a laboratory X-ray source, this technique clearly requires the availability of a high performance synchrotron source. The particular variant of X-ray absorption spectroscopy to be discussed here, near-edge X-ray absorption fine structure spectroscopy (NEXAFS) was devised in the 1980s. The technique, which occasionally is also referred to as X-ray absorption near edge structure (XANES), was developed in order to provide information on the electronic and geometric structure of molecules bonded to solid surfaces, mostly that of metals. The method has had its largest success when applied to low Z molecules (Z is the atomic number), for which intense absorption edges are located in the soft X-ray region (100–700 eV). This is not a severe restriction, most organic molecules consisting of light atoms such as carbon, nitrogen, oxygen and fluorine, can be investigated in a straightforward fashion by using photons in this energy region [1]. In its standard variant the techniques probes transitions from a K-edge (the deepest core shell) of an atomic species into

unoccupied molecular orbitals. As a result the technique is sensitive not only to ones of intramolecular character present in the molecule before adsorption on the surface, but also to interactions between the molecule and extramolecular atoms, e.g. surface atoms. A particular advantage of the method over other photoelectron spectroscopy variants which are sensitive to molecular orbitals, in particular, over ultraviolet photoelectron spectroscopy (UPS), is that the molecular orbitals detected with NEXAFS are selected as regards contribution of a specific type of atoms, e.g. carbon or nitrogen atoms. The huge background from the metal substrate typically governing UPS data is directly removed, making the analysis of experimental data considerably more straightforward.

Compared to other techniques which are used to gather information on the electronic and geometric properties of ultrathin molecular layers supported by solid substrates, e.g. methods employing vibrational spectroscopy, infrared spectroscopy (mostly used under grazing incidence, – infrared reflection adsorption spectroscopy (IRRAS)) or electron energy loss spectroscopy (EELS) as well as other photoelectron spectroscopy based methods, NEXAFS has several advantages. First, it can be applied in a rather straightforward fashion, data analysis is fast and does not require sophisticated considerations. Secondly, charging problems as often encountered in XPS and UPS applied to insulation substrates, are a problem only in rare cases. Finally, the transition dipole moment (TDM) governing the electronic excitations can be oriented both normal and parallel to a metal surface to allow for a detection of the corresponding resonance, in contrast to infrared spectroscopy (and EELS carried out in the dipole scattering regime) where only transition dipole moments orientated perpendicular to the surface can be probed. NEXAFS is also rather sensitive, investigations for small adsorbate coverages substantially below one monolayer can be carried out in a routine fashion.

Before describing the properties of NEXAFS spectroscopy in more detail we will briefly address the two most important variants of photoelectron spectroscopy which can be carried out with laboratory sources, X-ray photoelectron spectroscopy (XPS) and ultraviolet photoelectron spectroscopy (UPS). These two techniques allow to determine the binding energies of occupied states in the core-level region (XPS) and the valence-band region (UPS), respectively.

The photoelectron spectra consist of peaks corresponding to the direct, primary excitation and a background caused by secondary processes, including Auger decays within the core as well as inelastically scattered electrons. Even slight charging of the samples generates severe problems in data analysis and special precautions need to be applied to avoid spurious shifts of peaks or the appearance of artifacts, e.g. a charge compensation using the second electron source or in some cases even a second photon source. A striking advantage of NEXAFS when applied to insulating substrates such as diamond and polymers is that charging effects are, in principle, absent since the absorption of incident photons is detected. Of course, when the X-ray absorption is detected via the

monitoring of the secondary electron yield (partial electron yield or Auger yield, see below) a substantial charging of the sample has to be avoided. Experience has shown, however, that there are only few substrates (e.g. mica) where charging causes severe problems. On most other insulating substrates, including thin polymer films and diamond substrates, no substantial problems are encountered, small charging of up to 10 eV do not cause major problems in the electron-yield based detection of photon absorption.

With regard to investigating organic molecules a clear advantage of NEXAFS is the very high sensitivity towards the chemical nature of intramolecular bonds. For example, the C1s level binding energies as determined by XPS for carbon atoms in either a fully saturated hydrocarbon or in an aromatic compound such as benzene differ by $\sim 0.1\,\mathrm{eV}$ only. This value is often below the resolution of the electron energy analyzer available at the experimental setups. Even if this energy resolution is available, a careful calibration of the energy scale is required [2]. As a result, an unambiguous distinction between single and double bonds is a major challenge in XPS. In contrast to XPS, where the binding energy of the initial state is measured, NEXAFS is sensitive to the position of the final state as well. As a result the pronounced differences in energy of unoccupied σ^*- and π^*-orbitals cause features separated by several electron-volts in the corresponding NEXAFS spectra which makes the detection of double bonds rather straightforward.

These facts make the NEXAFS technique particularly well suited for following chemical modifications within ultrathin organic layers, e.g. as a result of a reaction with a substrate or a reaction between adsorbed molecules. Note, however, that, in contrast to XPS, NEXAFS is not quantitative, i.e. a direct determination of the sample stoichiometry or the relative ratio of σ- and π-bonded C atoms cannot be easily carried out. For that reason a combination of XPS and NEXAFS is recommended.

When it comes to a determination of the chemical nature and the orientation of the molecular species on a solid substrate the most important other technique is infrared (IR) spectroscopy and related techniques, like surface enhanced Raman spectroscopy (SERS) or sum frequency generation (SFG). The most striking advantage of these methods is that they can be employed as in-house techniques. With IR spectroscopy the vibrational spectra of adsorbed molecular species can be determined with the frequency of the vibrational bands being highly sensitive to the nature of intra- and intermolecular chemical bonds. While for metals the application of IR spectroscopy is straightforward for insulating substrates intensity problems render the detection of molecules adsorbed on single crystal surfaces rather difficult [3]. Only for normal incidence IR-spectroscopy can be applied to such semiconducting and insulating substrates in a straightforward fashion, however in such a case only vibrations with a transition dipole moment orientated parallel to the substrate can be seen [4]. Only recently a routine investigation of infrared vibrations on a solid oxide substrate has become possible [5]. When IR-spectroscopy is applied to metal surfaces, only vibrations with a transition dipole moment ori-

entated perpendicular to the surface can be seen in IRRAS, vibrations with a transition dipole moment parallel to the substrate are completely screened, leading to the so called surface selection rule in infrared spectroscopy [6]. In several cases the lack of sensitivity to such molecular vibrations with transition dipole moments orientated parallel to the surface have made a unique interpretation of experimental IR and EELS data sometimes difficult. If, e.g., a vibration of a diatomic species (e.g. O_2) cannot be seen it might imply either that the molecules is orientated with its axis aligned parallel to surface - or not present on the surface at all. This restriction is not present in NEXAFS. As a result of the high energy of the soft X-ray photons being located well above the plasmon energies of a metal, the screening by the metal electrons is ineffective and the orientation of the incident $\boldsymbol{E}$ vector can be chosen at will.

The present contribution describes the basics of the NEXAFS technique and the corresponding experimental setup. Selected examples of applications are given to demonstrate the breadth and the strength of this particular type of spectroscopy.

1.2 Theory background

An understanding of the various features observed in NEXAFS spectra on a solid theoretical basis is a prerequisite for the use of NEXAFS as a reliable tool to investigate electronic structures and molecular orientations. In the following, a brief and simplified description of the underlying electronic effects governing NEXAFS spectroscopy is given.

A NEXAFS spectrum reflects the dependence of the photoabsorption cross section on the photon energy for values from just below the core level ionization threshold up to around 50 eV above. For the (over)-simplified case of an electron located in a single bound state (core level) and in the absence of any other empty electronic states the variation of the photoabsorption cross section when scanning the photon energy across the ionization energy would resemble a step function (the thick dashed line in Fig. 1.1c). For photon energies below the core electron binding energy no absorption would take place, whereas for photon energies above the ionization threshold an excitation of the core electron into the continuum of final states (plane waves describing an electron travelling away from the core hole) makes an absorption of photons possible.

Even for a free single atom (Fig. 1.1a), however, the measured cross section looks considerably more complicated. This is a result of the fact that there are considerably more final states than in the oversimplified model referred to above, the presence of the electrostatic potential of the atom's positively charged nucleus gives rise to a number of empty electronic states, located below (bound states) as well as above (unbound states) of the ionization threshold. The bound states can be roughly divided into valence state localized in the proximity of the core and Rydberg states with binding energies

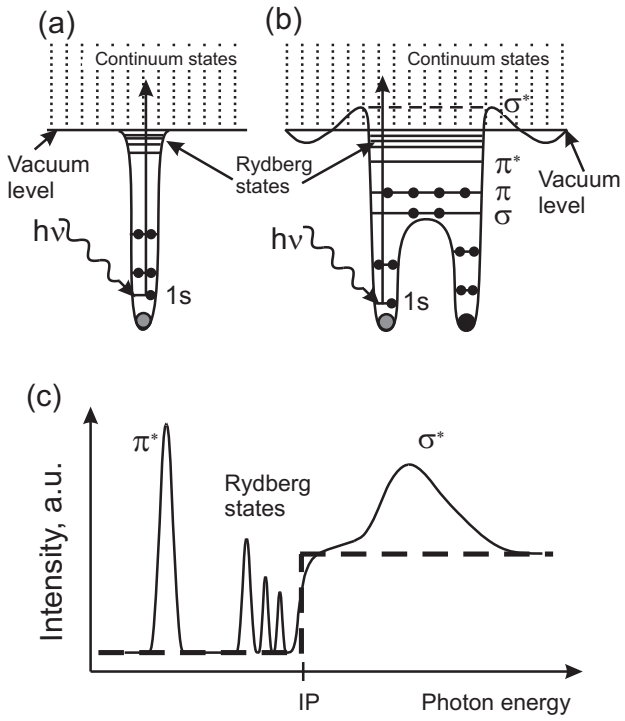

Fig. 1.1. (**a**) Schematic potential for isolated atom; (**b**) Schematic potential of a diatomic molecular (sub)group. In addition to Rydberg states and a continuum of empty states similar to those expected for atoms, unfilled molecular orbitals are present, which is reflected in the absorption spectrum (**c**). The thick dashed line corresponds to the photoabsorption cross section of an electron located in a single bound state (core level).

converging to the ionization threshold. Note, however, that in some cases this distinction is problematic [7]. The unbound states mostly correspond to excitations into (molecular) antibonding states and are located well above the ionization threshold, a typical feature of NEXAFS resonances arising from excitations into such states is the large energetic half-width.

A cartoon showing schematically the origin of NEXAFS features for the case of a diatomic unit is provided in Fig. 1.1b. The effective electrostatic potential and the corresponding K-shell spectrum are also shown. Around the ionization threshold, resonant transitions are superimposed on the step-like absorption edge as shown in Fig. 1.1c. Empty molecular orbitals are labelled as σ^*- and π^*-orbitals according to their symmetry. The lowest unoccupied molecular orbital (LUMO) of a π-bonded diatomic subunit of a molecule is usually a π^*-orbital, while σ^*-orbitals are found at higher energies (see Fig. 1.1c). The latter are most often found above the vacuum level for the

neutral molecule. Of course, an 1s $\rightarrow \pi^*$ transition or π^*-resonance can only be observed for molecules with π-bonding, i.e. double and triple bonds or aromatic systems, but not for single bonds.

The measured width of a resonance is determined by the resolution of the instrument (resulting in a Gaussian lineshape), the lifetime of the excited state (resulting in a Lorentzian lineshape), and the vibrational motion of the molecule leading to an unsymmetrical broadening [8]. Broadening due to the lifetime of a π^*-resonance is generally very small, on the order of a about 100 meV for e.g. the C1s $\rightarrow \pi^*$ excitation in benzene. Essentially, the final state lifetime is determined by the re-filling, or the decay of the core-hole pair, either by the excited electron falling back or by an Auger-transition involving other electrons. Transitions into unoccupied orbitals of σ-symmetry which are found at higher energies above the ionization threshold are energetically considerably broader, indicating strongly reduced lifetimes for such cases. This experimental finding can be rationalized by considering that the large overlap of these states with continuum states will, of course, strongly decrease the lifetime of these states. As a rule of thumb, the higher the resonance lies in the continuum the larger is its linewidth.

Rydberg orbitals give rise to sharp but weak resonances occurring below the ionization threshold. They are generally located between the π^*-resonance and the ionization potential. In the condensed phase or for strongly chemisorbed molecules, pure Rydberg resonances are quenched because of the large spatial extent of these electronic states. A clear separation is, however, not always possible. E.g. in the case of single CH bonds, a mixing of Rydberg orbitals with hydrogen-derived antibonding orbitals of the same symmetry leads to hybridization, thus increasing the intensity of the corresponding NEXAFS resonance located just before the C-K edge [9,10]. Finally, NEXAFS spectra can also exhibit multi-electron features, such as so-called shake-up structures, which can be associated with the indirect excitation of "passive" electrons. The sudden creation of the core hole potential induced by absorption of an X-ray photon by the "active" electron may knock one or more of the "passive" electrons into excited states. It is necessary to mention that in photoemission spectra the satellites are observed at lower kinetic energy than the main active-electron peak, but in X-ray absorption shake-up features are observed at higher photon energy than the primary resonance [1].

In addition to the information on the electronic structure of molecules or molecular fragments, NEXAFS can be used to determine the orientation of a molecule relative to the substrate surface. Bonds and the corresponding molecular orbitals are highly directional and the spatial orientation of an orbital, i.e. the direction of maximum orbital amplitude on the excited atom, determines the angular dependence of the K-shell spectra. Therefore, the transition intensities depend on the orientation of the electric field vector relative to the orientation of the molecule. Exploiting the polarization characteristics of synchrotron radiation (for a simplicity, we will assume that the radiation is linearly polarized), the orientation of a molecular orbital can be found by

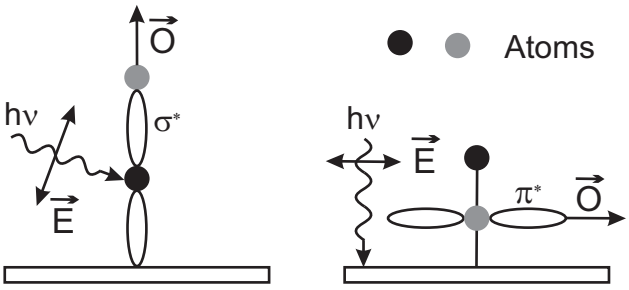

Fig. 1.2. Schematic representation of the origin of the angular dependence of NEXAFS resonances for a π-bonded diatomic molecule adsorbed with its molecular axis normal to the surface. As a result of the different overlap between the electric field vector $\boldsymbol{E}$, and the direction of the final state orbitals $\boldsymbol{O}$, the π^*-resonance is maximized at normal incidence (right), while the σ^*-resonance is maximized at grazing incidence (left).

determining the intensity of the corresponding resonance as a function of the incidence angle of the photons, θ. The quantum mechanical description of the excitation process for a single electron in the dipole approximation leads to an equation relating the initial state Ψ_i and the final state Ψ_f to the photoabsorption cross section σ_x:

$$\sigma_x \propto | < \Psi_f | \boldsymbol{e} \cdot \boldsymbol{p} | \Psi_i > |^2 \rho_f(E) \tag{1.1}$$

with $\boldsymbol{e}$ being the unit electric field vector, $\boldsymbol{p}$ the dipole transition operator, and $\rho_f(E)$ the density of final states [1]. In the case of linearly polarized light, the angular dependence of the matrix element of interest $| < \Psi_f | \boldsymbol{e} \cdot \boldsymbol{p} | \Psi_i > |^2 = |\boldsymbol{e} < \Psi_f | \boldsymbol{p} | \Psi_i > |^2$ assumes a simple form and the expression $< \Psi_f | \boldsymbol{p} | \Psi_i >$ is known as transition dipole moment (TDM). For a 1s initial state and a directional final state orbital the matrix element $|\boldsymbol{e} < \Psi_f | \boldsymbol{p} | \Psi_{1s} > |^2$ points in the direction of the final state orbital $\boldsymbol{O}$ and the transition intensity becomes

$$I \propto |\boldsymbol{e} < \Psi_f | \boldsymbol{p} | \Psi_{1s} > |^2 \propto |\boldsymbol{e} \cdot \boldsymbol{O}|^2 \propto \cos^2 \delta \tag{1.2}$$

with δ being the angle between the electric field vector $\boldsymbol{E}$ and the TDM direction. Therefore, the intensity of a resonance is largest when the electric field vector $\boldsymbol{E}$ lies along the direction of the final state orbital $\boldsymbol{O}$ (or the TDM direction), as schematically shown in Fig. 1.2, and vanishes when $\boldsymbol{E}$ is perpendicular to it. Note that σ^*-orbitals have a maximum orbital amplitude along the bond axis while π^*-orbitals have maximum amplitude normal to the bond direction (Fig. 1.2). In the case of molecules with π-bonds, the large π^*-resonance is most suitable for a quantitative evaluation of the angular dependence because of its clear separation from the ionization step and the absence of any interfering background.

In common case, the TDM direction can be described through a polar angle α and an azimuthal angle ϕ and in equations for angle dependencies of

resonance intensities there is a dependence both on α and on ϕ [1]. It means for the determination of the molecule orientation it is necessary to measure at least two series of NEXAFS spectra at two different azimuthal sample orientations. Fortunately, the azimuthal dependence is eliminated in many cases by the symmetry of the surface. The surface symmetry established several equivalent in-plane chemisorption geometries which lead to the formation of adsorbate domains. Thus for molecules adsorbed on a surface with an at least three-fold symmetry, there is an averaging over the azimuthal angle ϕ and the NEXAFS resonance intensities can be expressed as:

$$I \propto P\cos^2\theta(1-\frac{3}{2}\sin^2\alpha)+\frac{1}{2}\sin^2\alpha\,, \tag{1.3}$$

where P denotes the degree of polarization of the incident X-ray light. This equation is quite simple and it is routinely used for a determination of the molecular orientation.

Equation 1.3 could be also written in the form

$$I \propto P\cos^2\theta(\cos^2\alpha+\frac{1}{2P}\tan^2\theta\sin^2\alpha) \tag{1.4}$$

and it is clearly seen that at the incidence angle $\theta = \arctan(\sqrt{2P})$ the absorption intensity does not depend on the molecule orientation. Taking in to account that $P \approx 1$, this angle θ is about 55° and it is known as "magic angle". The absorption intensity measured at this angle is very important for data analysis, because it allows to determine a scaling factor, which contains all physical and experimental constants. Usually for samples without any preferable orientation of molecules it is enough to record NEXAFS spectra only at this "magic" angle.

Another useful consequence of (1.3) is a presentation of the difference of intensities measured at two different angles, namely at normal (90°) and gracing (20°) incidence. Taking in to account that $\cos 90° = 0$ and $\cos 20° \approx 1$ we obtained:

$$I(90°) - I(20°) \propto (\frac{3}{2}\sin^2\alpha - 1). \tag{1.5}$$

Here α is the angle between the electric field vector $\boldsymbol{E}$ and the TDM direction averaged over azimuthal angles ϕ. This difference spectra is known also as a linear dichroism and it is negative for small α and positive at $\alpha \geq 55°$. According to Fig. 1.2, if molecule have double/triple bonds in its molecular plane the negative dichroic signal of π^*-resonances corresponded to these bonds will result in a flat orientation of the molecule and positive one to upright-oriented molecules. Since σ^*- and π^*-orbitals are normal to each other, the dichroic signal of σ^*-resonances has the opposite sign than for π^*-resonances.

As an obvious case, we presented the results obtained by Fuhrmann et al. [11] on the determination of the molecular orientation of ethylene adsorbed on Cu(111). C_2H_4 was adsorbed at temperature of 100 K and the NEXAFS spectra were recorded at grazing and normal incidences. They are presented

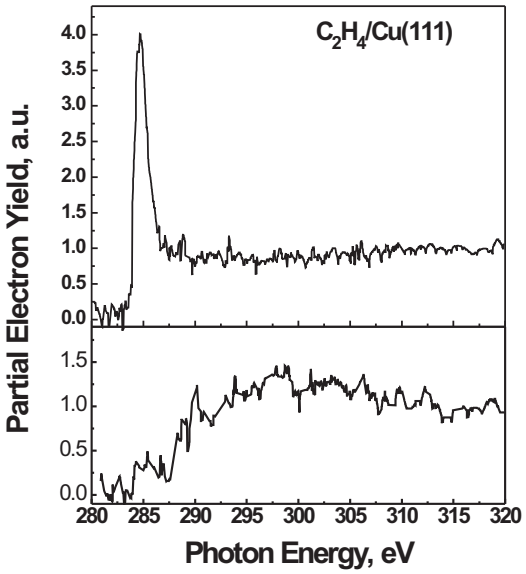

Fig. 1.3. NEXAFS spectra recorded at normal incidence (lower panel), and at grazing incidence (upper panel) for monolayers of ethylene adsorbed on Cu(111) at temperature of 100 K.

in Fig. 1.3 and the absence of π^*-resonance at E = 284.7 eV for normal incidence (Fig. 1.3, lower panel) clearly demonstrate a flat orientation of ethylene molecules adsorbed on Cu(111).

A rather reliable basis for the assignment of the features in the experimental NEXAFS spectra can be provided by a series of calculations with a quantum chemistry program package, e.g. the StoBe (Stockholm–Berlin) package [12]. Note that StoBe allows to compute and analyze the electronic structure as well as spectroscopic and other properties of molecules. A particular advantage of this program is that due to the use of density functional theory (DFT) methods it can deal with rather large molecules, e.g. hexa-perihexa-benzocoronene with 42 carbon atoms and 18 hydrogen atoms represents no major problem. Also atomic clusters can be handled in a straightforward fashion. The approach is based on self-consistent solutions of the Kohn–Sham equations using a linear combinations of Gaussian type orbitals and it can produce the projection intensity of the core-π^* transition according to the molecular symmetry and the sum of these projections will give rise to the final NEXAFS spectra. The theory and numerical details of the realization can be found in [12–15]. The striking advantages of using the results of such theoretical calculations with regard to the interpretation of features in expe-

rimental NEXAFS data will be demonstrated for selected cases in Section 1.4.

1.3 Experimental method and setup

The key feature of NEXAFS spectroscopy with regard to other variants of photoelectron spectroscopy is the fact that the resolution of the method is not determined by the energy analyzer used to determine the kinetic energy of the photoexited electrons. Since the measured quantity, measured either directly or indirectly, is the absorption of X-rays, the energy resolution is only determined by the employed monochromator.

The most straightforward way to measure the X-ray absorption cross section would be to measure the attenuation of a direct beam of X-ray photons transmitted through a sample using an X-ray sensitive detector. This method can be easily applied only for rather thin samples since the penetration depth of X-rays is in the μm- to mm-region (depending on incident energy). A striking disadvantage of such straightforward measurements would be the complete absence of any surface sensitivity.

In the most important variant of NEXAFS spectroscopy used today for the investigation of surface properties, the absorption of X-ray photons is measured by detecting the secondary electrons generated by the decay of the core hole emitted from the sample into the vacuum. While the most direct way to measure the total current would be to use a sensitive amperemeter to measure the total photocurrent indexPhotocurrent generated by the impinging photons as a function of photon energy, in practice it has proven more effective to measure the electrons emitted into the vacuum using electron multipliers or channel plates.

A typical NEXAFS experimental setup is presented in Fig. 1.4a. First, a monochromator is used to transmit only light with predefined energy which then hits the sample substrate. The shape of the beam is defined by a set of horizontal and vertical slits. A gold grid (typical transmittance 85%) is placed in the optical path making it possible to monitor the intensity of the X-ray photon beam incident on the sample. Although the current recorded for this gold grid cannot be used to directly determine the transmission function of the monochromator (see below) the recorded signal can be conveniently used for energy calibration purposes. The X-ray beam then enters the analysis chamber and hits the sample mounted on a special manipulator allowing to change sample orientation with respect to the incident beam (polar as well as in azimuthal angles).

As mentioned above the photoabsorption process taking place when the incident photons hit the sample substrate results in the creation of a photoelectron and a core hole. The hole is subsequently filled by another electron, the corresponding excess in energy is dissipated either radiatively by the emission

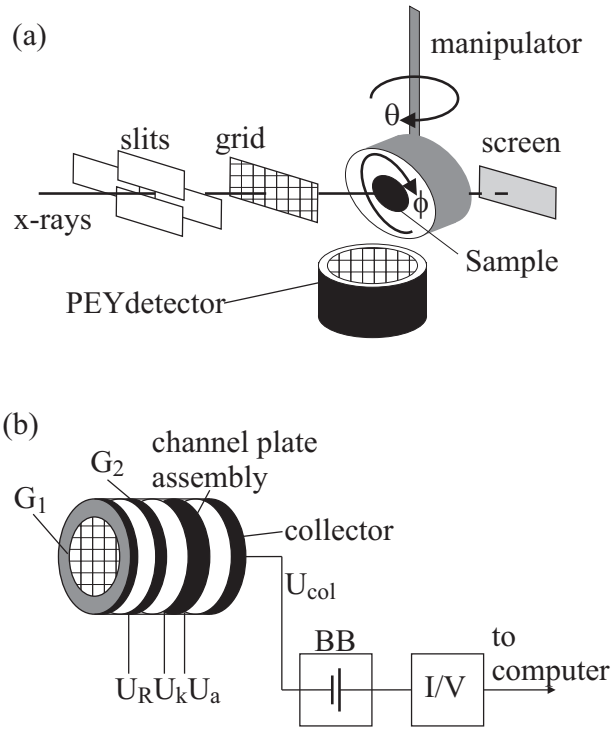

Fig. 1.4. (**a**) The scheme of the NEXAFS experimental setup; (**b**) the scheme of the PEY detector with corresponding electronics. G1 and G2 – two grids, BB – battery box, I/V – current amplifier; U_R, – retarding voltage,U_a and U_k – voltages on channel plates, U_{col} – voltage on collector.)

of a fluorescent photon, or non-radiatively by the emission of an Auger electron (see Fig. 1.5). Both channels are a direct result of the core hole created in the X-ray photoabsorption process and thus provide a basis to determine the absorption cross section. In principle, either dissipation process can be used for the detection. It is necessary to note, however, that for low-Z elements (C, N, O) the Auger electron yield is much higher than the fluorescence yield (FY), making the electron yield channel better suited for low-Z molecules [16]. In addition, electron detection provides the higher surface sensitivity and in the majority of studies published in the literature this so-called electron yield detection scheme has been employed. The reason for the higher surface sensitivity is the relatively low kinetic energy of the electrons and the corresponding mean free path in solid matter, which is typically less than 1 nm for energies between 250 eV and 600 eV [17]. The inelastic scattering process leads to an electron cascade, of which only those electrons with sufficient energy to overcome the work function of the material will escape the surface. The resulting effective escape depth and, therefore, the information depth of electron yield,

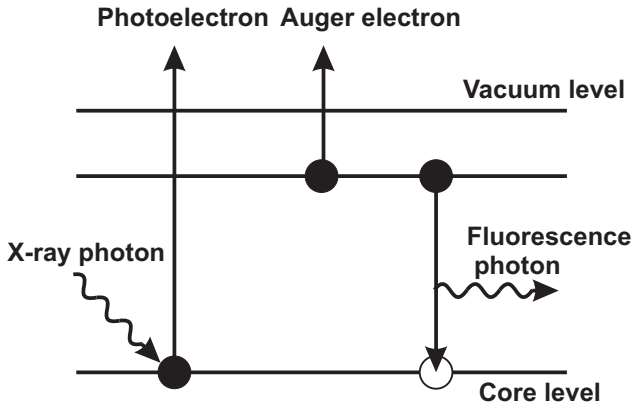

Fig. 1.5. The photoabsorption process including filling of the core hole by emission of a photon or an Auger electron.

has been estimated to be in the range of 5 nm for metals and semiconductors, and slightly larger for insulators due to the reduced electron-electron scattering mechanism [1]. The surface sensitivity can be further enhanced by applying a retarding voltage. By suppressing lower kinetic energy electrons, only those electrons that emerge from the outermost surface region (3 nm) are detected. For the investigation of adsorbates on surfaces, this so-called partial electron yield (PEY) detection has a better signal-to-background ratio than total electron yield (TEY) detection, where all electrons that emerge from the surface are detected. A further option is Auger electron yield (AEY) detection where only elastically scattered Auger electrons are recorded. The AEY mode provides the best surface sensitivity of the three detection techniques, but requires an electron energy analyzer. In the case of fluorescence detection, an appropriate detector has to be employed. In this contribution we do not discuss the FY detection method in detail, but note that this detection method is the one of choice for liquid and bulk samples, since in such environments the limited mean free path of photo- and secondary electrons makes the application of the PEY and TEY method impossible.

In Fig. 1.4b we show the typical design for a partial electron yield detector used for monitoring the absorption of the X-ray photons. The PEY detector is assembled using two high transmission metal grids for retardation, a double or triple channel-plate assembly for electron multiplication and a collector [18]. The first grid is usually grounded and the second grid is operated at retardation voltage -U_R, which rejects all electrons with energies less than U_R. Typically U_R is set to a value 100–120 eV less than the energy of the corresponding Auger peaks located at around 260 eV (C), 370 eV (N) and 510 eV (O). Electrons with the energies above U_R pass through these two grids and are then accelerated towards the channel-plate assembly by a small positive voltage ($U_a \approx 50$ eV) on the contact just before the upmost

channel plate – the anode. The electron signal is amplified by channel-plate arrangement by the application of a voltage ($U_k \approx 2000\,eV$) on the contact just behind the bottommost channel plate – the cathode. The double channel-plate arrangement operates at a total gain of 10^7-10^8 and the electron output is collected by a collector which is connected for current measurement to a floating battery box. This battery box supplies a low-noise positive potential (U_{col}) in the 2–3 kV range. The high potential is generated by a series of batteries which are suitable insulated from each other and the battery box housing and soldered together to eliminate noise. The achievable noise level is limited by leakage currents and is about 10^{-11} A. Normally, the collector voltage U_{col} is kept somewhat ($\approx 200\,eV$) larger than U_k. The negative side of the battery string is connected to the input of voltage/current amplifier which generates an output voltage proportional to the input current. With a gain of $10^7 - 10^8$ the output voltage will be in the range 0.5–5 V which fits quite well to corresponding interface card (A/D converter) of the computer. The computer must be also connected with the monochromator to control the energy of the incident X-ray photons. Note, that for a good signal-to-noise ratio of the electron yield signal the acceptance angle of PEY detector should be as large as possible. Correspondingly, it should be positioned close to the sample. An alternative is the use of channel plates with large diameter.

Before recording NEXAFS spectra it is very important to precisely adjust the spot on the sample surface illuminated by the incident X-ray photons, since contributions e.g. from the sample holder to the measured signal will make a proper analysis of the data impossible. In particular for gracing incidence the position of the sample has to be defined within a few tenth of a mm. In order to achieve such a proper alignment and to avoid contributions from unintentionally illuminated parts of the experimental setup it is quite useful to employ a phosphor-covered test sample and a phosphor-covered screen behind the sample-holder. Fluorescence in the visible regime will then allow for a good alignment of the manipulator and the whole chamber.

To extract quantitative information about adlayers on a substrate raw NEXAFS spectra recorded at different angles of incidence have to be properly normalized. We typically apply the following procedure: first, the constant background signal, present without illumination (dark currents) is subtracted from the spectra. Then the spectrum recorded for the clean substrate is subtracted from the adlayer spectra. The resulting data is then divided by a spectrum recorded for a freshly sputtered gold film to compensate the energy dependence of the transmission function of the beamline. Finally, the intensities are normalized to an edge jump of 1, i.e., intensity difference between 275 and 330 eV in a case of C K-edge. This procedure provides information exclusively on the adsorbed layer. There is also a series of another normalization procedures (see [1]) and in dependence on a sample a proper processing has to be used.

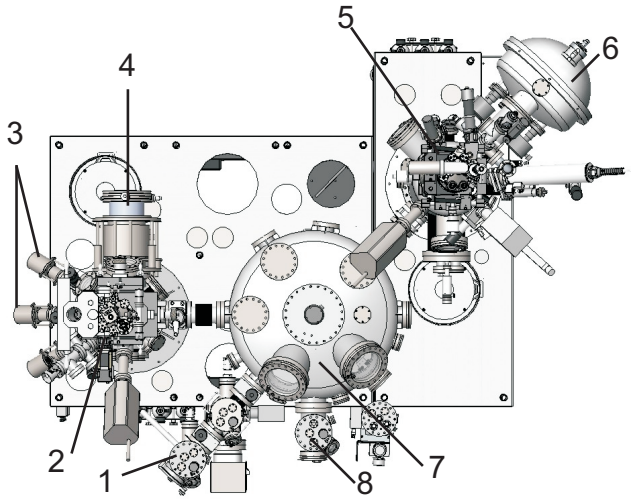

Fig. 1.6. The drawing of XPS/NEXAFS system (top view): 1 - load lock chambers, 2 - preparation chamber equipped by evaporators (3) and LEED system (4), 5 - analysis chamber with XPS/UPS electron analyzer Scienta R3000 (6), 7 - distribution chamber with park-station (8), which serves for keeping samples under UHV-conditions for long time.

Experimental NEXAFS system

The apparatus used by us to measure NEXAFS spectra is additionally equipped with complimentary surface analytical techniques, namely XPS/UPS, low energy electron diffraction (LEED) and thermal desorption spectroscopy (TDS). Especially for more complex systems the possibility to characterize samples by other methods has been shown to be crucial for providing a unique and reliable interpretation of the experimental NEXAFS data. The scheme of such rather complex, multichamber UHV-system used by us is presented in Fig. 1.6. It consists of the analysis chamber (5) for NEXAFS/XPS measurements, the preparation chamber (2) equipped by evaporators (3), ion sputter guns and LEED system (4), a sample transfer system, including the distribution chamber (7) with the park-station (8) and two load lock chambers (1). One of the load lock chambers is designed for a use of a special transport box, which allows to transfer samples to another systems under UHV conditions. A crucial point is the sample transfer system which at the same time allows to carry out measurements in an extended temperature region. With the present setup samples can be investigated in a temperature region of at least 50–1000 K. This NEXAFS/XPS apparatus was designed and built by PREVAC (Poland) [19] and is operated at the HESGM beamline of synchrotron facility BESSY II (Berlin, Germany). A photo of the setup is presented in Fig. 1.7. Similar end-stations are installed at another synchrotron

Fig. 1.7. The view of XPS/NEXAFS endstation installed on HESGM beamline of synchrotron BESSY II in Berlin.

facilities, e.g. at MaxLab (Lund, Sweden), NSLS (Brookhaven, USA), ALS (Berkeley, USA), etc.

We would like to conclude this chapter by noting that the spatial resolution of NEXAFS is determined by the spot size of the X-rays on the surface and the acceptance area of the analyzer, and is usually macroscopic, i.e. the information obtained on the electronic structure and the molecular orientation will normally be averaged over a macroscopic (mm-sized) region.

1.4 Applications of NEXAFS spectroscopy

A detailed investigation of the fine structure at the adsorption edges of light elements such as C, N and O was first carried out in the 1980s for the case of "small" molecules such as CO and NO adsorbed on single crystal metal surfaces [20]. Since then NEXAFS has been used successfully to determine the electronic structure and molecular orientation of a fairly large number of molecules on many different substrates. The seminal book by Stöhr [1] provides an excellent overview of the basic principles of this technique and the results obtained until the early 1990s. In more recent reviews one can find reports on the application of the NEXAFS spectroscopy for the study of liquids and polymers [21] as well as for a study of inorganic samples, in particular, transition metal carbides and nitrides and other interstitial compounds [22]. In the present contribution we concentrate on the application of the NEXAFS technique for studies of functionalized surfaces and organic nanostructures. Rather than providing a broad overview of experimental studies carried out in the last years we will present a number of selected examples which demon-

strate the advantages of NEXAFS spectroscopy also to scientists new to this field.

1.4.1 Structural rearrangements at organic/metal interfaces

Distortion of C-H bonds in benzene adsorbed on metal surfaces

Over the past years a number of surface science studies of benzene adsorbed on a variety of close-packed metal surfaces have been reported [23–26]. The data consistently show that for coverages up to a monolayer, benzene adsorbs with its symmetry plane parallel to the substrate. In the case of transition metal surfaces with a significant fraction of the d-bands unoccupied the interaction of the benzene system with the substrate atoms results in the formation of a stable chemical adsorbate-substrate bond. The NEXAFS spectra of physisorbed and chemisorbed benzene are strongly modified with respect to gas phase spectra. These changes arise from physical (final state effects, screening of the core hole by the metal substrate) as well as from chemical (changes of electronic structure as a result of the benzene-metal bonding) interactions. The precise origin of these differences is not completely understood and has remained to some extent controversial, although the benzene-metal adsorption system is among the most extensively adsorbate systems studied. As demonstrated in a study by Weiss et al. [27] the strongest modifications in the NEXAFS spectra can be observed for the benzene π^*-resonance which is found to be significantly broadened with respect to the gas phase even in the case of physisorption on the most inert metal, Au. In this study NEXAFS spectra of benzene adsorbed on different metal surfaces, Au(111), Rh(111), Pt(111) and Ru(0001) were measured and it has been demonstrated that a detailed analysis of the dichroism seen for NEXAFS resonances provides direct information on the adsorption induced out-of-plane bending of C-H bonds [28].

The NEXAFS spectrum recorded at the C1s edge for a thick (d>10 nm) benzene multilayer as shown at the top of Fig. 1.8 is very similar to the gas phase spectrum of benzene observed by Horsley et al. [23]. Peaks 1 and 3 correspond to π^*-resonances, peaks 4 and 5 correspond to σ^*-resonances. The weak feature at about 287.5 eV labelled 2 is assigned to a Rydberg resonance. For a more detailed assignment of the various resonances the reader is referred to [27].

In the lower part of Fig. 1.8 we display angle-dependent NEXAFS spectra recorded for benzene monolayers adsorbed on Au(111), Rh(111), and Pt(111) at normal and grazing photon incidence under the same experimental conditions. For the Au(111) surface the benzene NEXAFS spectra show a strong angular dependence. This strong linear dichroism is expected, since benzene adsorbs with its molecular plane parallel to the Au-substrate surface (Fig. 1.9, upper panel). In particular from the fact that the intensity of the π^*-resonance recorded at normal incidence its virtually zero it can be concluded that the benzene basically retains its gas phase structure, in particular the tilt of the

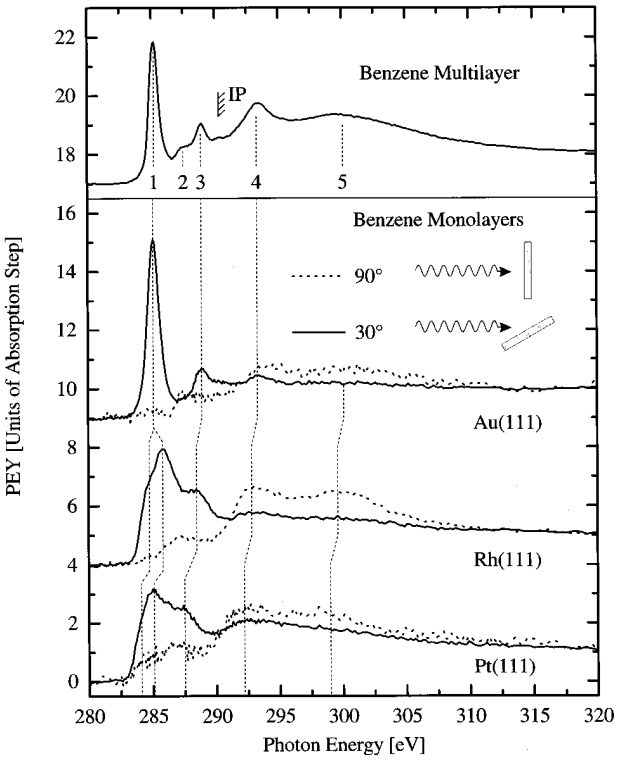

Fig. 1.8. NEXAFS spectrum of a benzene multilayer at 120 K (top). Polarization dependence of NEXAFS spectra recorded for benzene monolayers adsorbed on Au(111), Rh(111) and Pt(111) (bottom). The spectra were recorded for normal (90°) and grazing (30°) photon incidence. The hatched line at 290.3 eV indicates the ionization threshold. (Reprinted with permission from K. Weiss, S. Gebert, M. Wühn, H. Wadepohl, Ch. Wöll, Journal of Vacuum Science and Technology A **16**, 1017 (1998) Copyright (1998) American Vacuum Society.)

C-H bonds away from the molecular plane must be much smaller than in the case of transition metals with only partially filled d-bands, see below.

The spectra of benzene monolayers strongly chemisorbed on Rh(111) and Pt(111) are similar to spectra reported earlier for benzene chemisorbed on Pt(111) [23]. In contrast to the spectra recorded for benzene monolayers on Au(111) several pronounced differences can be observed between the monolayer and multilayer spectra. The most conspicuous feature is the strong broadening of the π^*-resonance. This splitting of the π^*-resonance is attributed to a hybridization of the benzene π-orbitals with metal electronic states leading to the formation of several different hybrid electronic states with contributions from both, C atomic orbitals and empty states in the metal conduction band, as discussed by Stöhr [1]. This hybridization (or mixing) of molecular

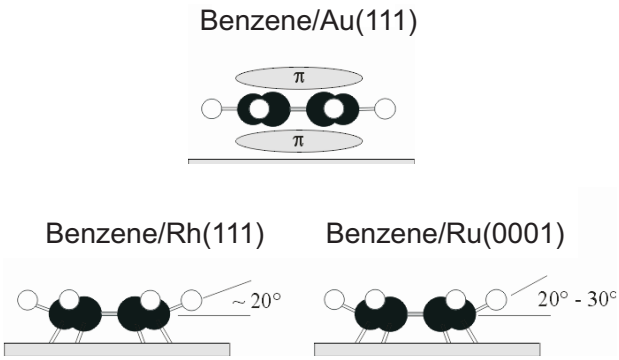

Fig. 1.9. Schematic models of benzene molecule absorbed on Au(111), Rh(111) and Ru(0001).

(or atomic) orbitals with metal states leads to a strong decrease of the final state lifetime and thus explains the significant increase in linewidth when going from the multilayer to the monolayer.

The spectra recorded at normal incidence for the chemisorbed benzene species on Rh(111) and Pt(111) show considerable intensities for the π^*-resonance. At first this experimental finding seems to indicate a tilted adsorption geometry since for a perfectly flat orientation of the benzene molecular plane with regard to the substrate the intensity of the π^*-resonance should be strictly 0 at normal incidence, as observed for the case of Au(111) (see above). Chemical intuition as well as the results obtained by other techniques strongly suggest, however, that the CCC plane of benzene is orientated largely parallel to the surface on both, Rh(111) [29] and Pt(111) [30]. A more detailed investigation of the binding situation has revealed that the rather pronounced residual intensity of the π^*-resonance at normal incidence can be related to conformational changes resulting from the formation of chemical bonds between the carbon atoms and the transition metal substrate. The rehybridization of the carbon π^*-orbitals from sp^2 (in benzene) to sp^3 results in a pronounced change in the orientation of the transition dipole moment governing the excitation of the C1s core electron into the empty molecular orbitals. These electronic changes are accompanied by a pronounced bending of the C-H bonds away from the C-C-C plane, (see Fig. 1.9, lower panel). In a very simplified picture these adsorption induced distortions can be explained in terms of interfragment interaction, since the C-H bond bending away from the metal surface maximizes the overlap between the orbitals of benzene and the electronic states of the metal. For a detailed discussion of the implications of such a distortion of the NEXAFS spectra see [27, 28].

Charge-transfer-induced rearrangements of tetracyano-p-quinodimethane on Cu(100)

Tetracyano-*p*-quinodimethane (TCNQ) is one of the strongest organic electron acceptors and has long been regarded as a prime candidate for the formation of organic/inorganic charge-transfer compounds [31]. The interface between TCNQ adsorbate and a Cu substrate can thus be considered a model system for the interfaces between the strong organic acceptors usually involved in organic light-emitted diodes or organic solar cells and the metallic contacts.

In a recent paper [32] a combination of different experimental techniques supported by theoretical calculations has demonstrated that the donation of an electron from the substrate to the TCNQ molecules leads to a molecular conformation very similar to the well-documented structure of the corresponding anion or the dianion in solution. The conformation of the negatively charged (or anionic) molecule results in a rather strong bonding between the nitrogen lone pairs and the copper atoms at the surface. A more detailed theoretical investigation revealed that this interaction is rather localized, so that the surface atoms bonded to the cyano groups are significantly lifted (or bent away) from their usual positions at the surface.

The main features that determine TCNQ acceptor functionality are the four peripheral cyano groups and the central hexagonal ring. In its neutral form the hexagonal ring is not aromatic and the molecular conformation is very rigid owing to the alternation of multiple and single bonds (*p*-quinoid character). Upon transfer of one electron, however, the central hexagon ring is aromatized which can only take place by changing the character of the bond between the hexagon ring and the dicyanomethylene group from double to single. The extra electron is thus accommodated in one of the peripheral nitrogen atoms, so that one of the molecular ends remains radical in character, whereas the other end loses the radicaloid character by accumulating one extra electron. Bond conjugation at the dicyanomethylene ends, however, remains, so that both the extra electron and the radical character are delocalized at each dicyanomethylene group. The dianion form of TCNQ is also well known: in this case the second electron transferred to the molecule is accommodated at the radicaloid dicyanomethylene end. In the anionic and dianionic forms, bond conjugation is restricted to the central ring and to the dicyanomethylene groups: the terminal carbon of bond between the hexagon ring and the dicyanomethylene group now has a higher sp^3 character and, consequently, the cyano groups bend away from the molecular plane.

As demonstrated by the angle resolved results presented in [32] NEXAFS spectroscopy is ideally suited to monitor the conformational and bonding changes accompanying the adsorption TCNQ on a Cu(100) surface. An investigation of the N1s spectra reveals that the peak assigned to the CN group is split, in contrast to NEXAFS spectra measured for TCNQ powder where only a single resonance is observed. The CN group has two orthogonal π^*-orbitals and for the neutral molecules the energies are very close thus re-

sulting in a single peak only. However, upon adsorption on the Cu-substrate, the strong interaction of the CN groups with the Cu(100) substrate leads to a pronounced increase of this splitting, resulting in two separate peaks. Their angular dependencies of these two different contributions were analyzed by a fit procedure according to (1.3) yielding tilt-angles of 19.7° and 10.0° for the low-energy and high-energy peaks, respectively. Together with the C1s analysis, it was concluded that TCNQ adopts a planar, flat-lying adsorption geometry on Cu(100), with the CN groups tilted away from the surface by an angle of $15 \pm 5°$.

These results exemplify the fundamental role that charge-transfer processes across metal-organic interfaces have on molecular self-assembly and subsequent crystal growth. Such a charge transfer modifies the energy level alignment at the interface, but they also affects molecular conformation and, thereby, adsorbate self-assembly. These results also demonstrate that in case of strong bonding between a metal surface at a molecular substrate the static surface approximation may no longer be applicable: substrate reconstruction and surface-mediated interactions must be explicitly taken into account. Predictions based on gas phase geometries of the molecules and corresponding intermolecular interactions may yield a poor description of the experimental results only.

1.4.2 Internal twist structure in aromatic self-assembled monolayers

Since the first systematic investigation of self assembled monolayers (SAMs) started about 25 years ago [33], this field has developed into an important section of research in the field of nanotechnology (see [34–36] and references provided there). The huge diversity and the enormous potential of these organic thin films continue to drive a number of new developments. In earlier work mainly alkanethiols have been used for the formation of SAMs on gold surfaces to unravel fundamental aspects of film formation, structure and properties. In later years aromatic organothiols have attracted an increasing amount of attention because of the higher rigidity of their molecular backbone and also because of the more interesting electronic properties of the conjugated π-systems. Today, an important application of SAMs is to create organic surfaces exposing predefined functionalities. Attaching an appropriate moiety to the monomers from which the SAM is fabricated allows tailoring the wettability and the reactivity of the organic surfaces exposed by the SAMs. Such organic surfaces have numerous potential applications in molecular electronics, electrochemistry and biochemistry [37]. A recently established, exciting new field based on SAM-modified substrates is interface-based supramolecular chemistry, where organic monolayers are used as templating substrates to anchor and grow highly porous materials like metal-organic frameworks (MOFs) [38–40].

Pyridine-terminated SAMs represent a particularly interesting type of organic substrates. An interesting result is described in a recent paper [41], where such pyridine-terminated organic surfaces have been used to enhance the rate of heterogeneous electron transfer between electrodes and the solution-phase of biological species. Recent studies have revealed that the chemical activity of pyridine-terminated SAMs is quite complicated [42, 43] and their properties cannot be predicted in a straightforward fashion from the properties of pyridine in solution.

NEXAFS spectroscopy is particularly well suited for the investigation of SAMs. An interesting example has been provided in [44] where it has been demonstrated the potential of the method for the case of a series of four related pyridine-terminated thiols with backbones comprising both aliphatic and aromatic parts. In this study the terminating pyridine-unit is followed by one (PPn) or two (PPPn) phenyl rings, where n=1–3 is the number of CH_2 groups separating the aromatic group and the thiol anchor. The schematic structure of one representative of this series of SAMs, namely PP1-SAM, is sketched in Fig. 1.10a.

In Fig. 1.10b C1s and N1s NEXAFS spectra recorded for PP1-SAM at different angles of incidence are presented. All spectra exhibit a number of characteristic absorption resonances which arise from excitations of C1s core electrons into unoccupied π^*- and σ^*-orbitals localized at the aromatic rings as well as into molecular orbitals of Rydberg character. Both carbon and nitrogen K-edge NEXAFS spectra reveal a pronounced dichroism, the strongest variations of intensity with angle of incidence are observed for π_1^*-resonances. The inset in Fig. 1.10b clearly demonstrate that the C1s $\rightarrow \pi_1^*$ transition consists of at least two components. This splitting of the C1s $\rightarrow \pi^*$ excitation is typical for pyridine and has already been observed in previous NEXAFS studies on pyridine [23, 45, 46] and other organic compounds containing pyridine moieties [42, 43]. Basically, this splitting is due to differences in electronic configuration of carbon atoms forming both phenyl and pyridine rings.

In principle, a determination of the tilt angle of the pyridine moieties can be carried out by analyzing the linear dichroism observed in the experimental data with the help of (1.3). When carrying out such an analysis, however, it has to be considered that the value for the angle α obtained from such analysis corresponds to an average of the tilt angles of the TDMs of all aromatic rings of the respective molecules (will below be referred to as "average tilt angle"). Therefore, the angle α_C determined from the carbon edge is an average value, and obtaining the value for a specific phenyl ring is not possible in a straightforward fashion. In contrast, the values α_N obtained from N K-edge dichroism corresponds to the tilt angle of the TDM of the pyridine moiety only (referred to below as "pyridine unit tilt angle"), since the other phenyl rings do not contain a N atom.

The TDM tilt angles obtained for the SAMs investigated in this study were found to be different for the different resonances, the average tilt angle amounts to 64–68° whereas to the pyridine unit tilt angle a value of 58–61° was

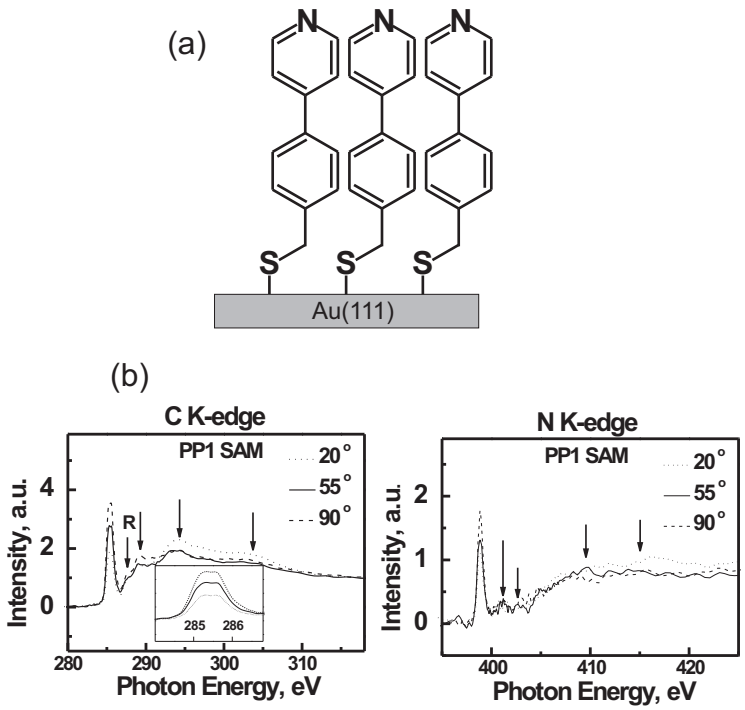

Fig. 1.10. (**a**) Schematic drawings of the PP1-SAM. (**b**) C K-edge and N K-edge NEXAFS spectra of PP1-SAM on Au(111) recorded at grazing incidence ($\theta = 20°$), the magic angle ($\theta = 55°$) and normal incidence ($\theta = 90°$) are displayed. The inset shows the region from 284-287 eV with the 1s $\rightarrow \pi^*$ transition that consists of at least two components.

found. These differences are considered significant and strongly indicate the presence of a non-planar conformation with substantial twist-angles between adjacent aromatic rings. For a given orientation of the molecular axis (described by the tilt angle β with respect to the surface normal) the TDMs of the 1s $\rightarrow \pi_1^*$ transition and, thus the average angle α, will depend on the rotation (or twist) of the aromatic ring with respect to the molecular axis, denoted by γ. Following this definition of the angles, the relationship between them is [1]:

$$\cos\alpha = \sin\beta\cos\gamma. \tag{1.6}$$

The values for α obtained from the analysis of the C K-edge and the N K-edge spectra will be different if the twist angle γ of the pyridine unit is different from the average of the aromatic moieties in the molecule, i.e. if the aromatic rings are twisted with respect to each other. The difference between the twist angles γ is equal to the internal twist angle ω of the aromatic rings. From detailed structural analysis for bulk crystals made from biphenyl and

several other oligophenyls it is known that typical values of the twist angle γ between adjacent phenyl unit in oligophenyl units amounts to about 15° at room temperature [47, 48]. For the free molecules, however, these values are much larger, e.g. for gas phase biphenyl a value of $40 \pm 5°$ has been reported [49]. The large twist angle for the free molecule results from the rather pronounced steric repulsion between adjacent H atoms. The huge differences between the twist angles in the bulk and the free molecule results from the fact that a reduction of the twist angle strongly increases the packing density, therefore upon crystallization the twist angle is strongly reduced. Clearly, the gain in crystallization energy overcompensates the steric repulsion between the H atoms. Unfortunately, in the case of pyridine-phenyl units no experimental information from the bulk structure analysis is available concerning the twist angle between the pyridine unit and the adjacent phenyl rings. For this reason we have carried out a geometry optimization using the the commercial quantum chemistry software package Gaussian [50]. The optimized geometry obtained from using this program package for the free PP1 molecule, yields a value of 36°, quite similar to that reported for free biphenyl molecules. [49]

In principle, the presence of a non-zero twist angle could, in addition to the changes of the linear dichroism governing the intensity of the individual resonances, also have a direct effect on the NEXAFS spectra. This expectation is based on the following consideration. Starting from a hypothetical planar conformation, a torsion of the phenyl unit with regard to the pyridine unit will reduce the coupling (mixing) of the π^* molecular orbitals of adjacent aromatic rings. As a result, for a given C atom, the ratio of intensities of transitions into final states localized at the ring containing the C atom under consideration to those into a final state localized at an adjacent ring will depend on the twist angle. To demonstrate this effect, NEXAFS spectra of PP1 were simulated using the software package StoBe [12] for different values of the torsion angle ω. The corresponding results are presented in Fig. 1.11 where they are compared with an experimental NEXAFS spectrum recorded at the magic angle $\theta = 55°$. The theoretical results reveal that there is indeed a substantial variation of relative NEXAFS intensities with the internal twist angle. Comparison of experimental PP1-SAM data and theoretical spectra shows the best agreement for an intermediate torsion angle of 18°. This analysis thus makes possible an independent determination of the twist angle ω between adjacent phenyl units.

The tilt angle β of the molecular axis of PP1 in respect to the surface normal can be estimated from the experimental values α_C and α_N using (1.6) and the relationship between the twist angles of the pyridine unit and the phenyl unit:

$$\gamma_{phenyl} - \gamma_{piridyne} = \omega \tag{1.7}$$

Assuming that the PP1 molecules chemisorbed on the Au surface actually have an internal twist angle of $\omega = 18°$ and considering that α_C is equivalent to the arithmetic average of the TDM tilt angles of the pyridine and the phenyl units, a value of 15° is obtained for the tilt angle β. This value is fully con-

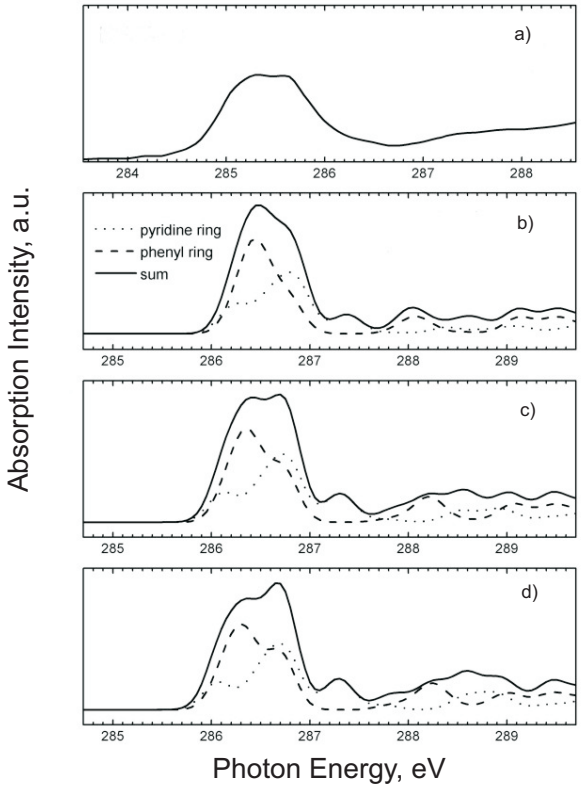

Fig. 1.11. Comparison of a) the experimental NEXAFS spectrum of the PP1-SAM on Au(111) recorded at the magic angle and NEXAFS spectra of PP1 molecules calculated using the StoBe program package. Spectra have been calculated for three different internal twist angles ω of the aromatic rings: b) 36°, c) 18°, and d) coplanar conformation ($\omega = 0°$). Both maxima of the π^*-resonance have contributions from C atoms both in phenyl and pyridine rings.

sistent with the other results obtained by other techniques (IR spectroscopy, XPS) as discussed in more detail in [44].

1.4.3 Coverage dependent orientation of terephthalic acid molecules on TiO_2(110)

Chemically functionalized surfaces play an important role in many nanotechnological applications. At present, most works concentrate on the adsorption of organic molecules on metal surfaces, only few attempts have been made so far to create a chemically functionalized metal oxide surface by adsorption of organic molecules, even though metal oxide surfaces provide anisotropy

and specific adsorption sites that could lead to well-ordered monolayers. Terephthalic acid (TPA) is a versatile molecular linker and has, consequently, received considerable attention with regard to the assembly of three-dimensional supermolecular frameworks stabilized by metal-carboxylate bonds [38–40], as well as in two-dimensional supramolecular architectures at surfaces [51–54]. In particular, TPA/TiO_2(110) is a promising system since one might expect the formation of an adlayer consisting of upright oriented molecules exposing an organic surface terminated by carboxyl groups. Such an organic substrate would have wide-ranging applications, similar to those of carboxyl-terminated SAMs [34]. Tekiel et al. studied the structure of a complete monolayer of TPA on TiO_2 by means of scanning tunneling microscopy and non-contact atomic force microscopy [55]. Their data was consistent with TPA adlayers with such an orientation perpendicular to the surface at a coverage of one monolayer (ML). This finding, however, is not consistent with the results of a recent ab-initio DFT calculations where it was concluded that the energetically most favorable orientation is one where the phenyl unit is oriented flat with regard to the TiO_2(110) surface [56]. Since micrographs obtained by scanning probe techniques, STM as well as AFM, do not allow for a direct determination of molecular orientation it is of pronounced interest to consider the results of a recent detailed NEXAFS investigation [57]. In this work, a coverage-dependent NEXAFS study of TPA adsorption and structure formation on a rutile TiO_2(110) surface has been presented. The orientation of the TPA molecules was determined from the dependence of the NEXAFS resonance intensities on the photon angle of incidence in case of the lowest (0.03-0.07 ML) and the highest (1 ML) coverages. In order to allow for a reliable analysis of the data, the measurements were carried out at $\theta = 20°, 30°, 55°, 70°$ and 90°, and at different azimuthal orientations of the TiO_2 crystal with azimuthal angles $\phi = 0°$ and 90° with respect to the $[\bar{1}10]$ direction of the (110) surface. Fig. 1.12a shows a series of carbon K-edge NEXAFS spectra taken for a TiO_2(110) substrate covered with 0.07 ML of TPA molecules. The set of spectra displayed in Fig. 1.12a shows a clear dependence of the peak intensities on the incident angle θ. In particular, the pronounced negative dichroic signal of the peaks at E=284.9 eV and E=285.5 eV, both assigned to the phenyl ring, and of the peak at E=288.3 eV, assigned to the carbonyl group in Fig. 1.12b, indicates almost flat lying molecules, in full agreements with the results of the theoretical calculations as discussed above.

A numerical fit of the experimental NEXAFS resonance intensities yields an average tilt angle of 18°. Ideally, for TPA molecules in a completely planar adsorption geometry, these peaks should vanish completely for $\theta = 90°$. However, TPA molecules adsorbed at step edges, defect impurities or dislocation sites might have a more tilted geometry and contribute to the NEXAFS signal as well [28]. In addition, a dynamic tilt angle resulting from the thermal occupation of the low energy vibrations of the molecule might also contribute, as was discussed for the case of benzene adsorbed on the same surface [58]. We thus conclude that the presence of a perfectly planar TPA adsorbate on

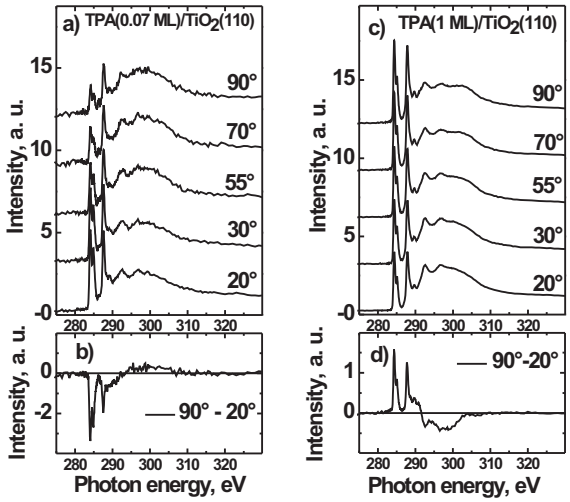

Fig. 1.12. Carbon K NEXAFS spectra for 0.07 ML (**a**) and 1 ML (**c**) of TPA coverage measured at different photon incidence angles. Difference of the spectra measured at $\theta = 20^\circ$ and 90° for 0.07 ML (**b**) and 1 ML (**d**), correspondingly.

the $TiO_2(110)$ surface would still be consistent with the average 18° tilt angle as determined from an intensity analysis of the corresponding NEXAFS resonances.

The NEXAFS spectra of the 1 ML sample in Fig. 1.12c show the same resonances as observed for the low-coverage 0.07 ML sample in Fig. 1.12a, however the dependence of the peak intensities on the photon angle of incidence is opposite already indicating a rather different molecular orientation of the TPA units. The difference spectrum reproduced in Fig. 1.12d demonstrates a positive signal for the π^*-resonances, a clear evidence of an upright orientation of the TPA molecules on TiO_2. Since the phenyl ring can rotate with respect to the carboxyl group, a random azimuthal orientation of the TPA molecules was assumed. On the basis of this model we obtain an average tilt angle the molecular axes with respect to the surface plane of $70^\circ \pm 10^\circ$. To summarize, this experimental study [57] revealed the presence of disordered, flat-lying TPA molecules at low coverages on the $TiO_2(110)$ rutile substrate. Upon increasing the coverage, a transition from flat-lying to upright-oriented molecules was observed.

1.5 Conclusions

Near edge X-Ray absorption fine structure (NEXAFS) spectroscopy has contributed significantly to a better understanding of the properties of interfaces

on the macroscopic as well as on microscopic scale, revealing detailed information on the electronic structure on the orientation of adsorbed molecules. As demonstrated by the examples discussed in this contribution today NEXAFS is a standard technique for obtaining direct information on the orientation and electronic structure of molecules within ultrathin layers supported by solids surfaces made from many different materials. The availability of computer codes allowing for a routine simulation of NEXAFS-spectra for small to medium-sized molecules (e.g. StoBe [12]), today make possible a straightforward interpretation of NEXAFS resonances. The major drawback of the method is the fact that experiments have to be carried out at a synchrotron, thus requiring travelling to such a large scale instrument. Today, due to the success of the technique, virtually all second and third generation synchrotrons provide NEXAFS end-stations equipped with transfer-systems. These systems make it possible also for users not familiar with this particular technique to carry out experimental investigations either on samples prepared at their home laboratories or on thin films prepared in situ under UHV-conditions. In connection with further developments we expect that this particular spectroscopy method will become even more popular. These new developments include small spot NEXAFS spectromicroscopy (better than 50 nm spatial resolution) and photoelectron microscopy where a NEXAFS contrast is used. [59] In addition, because of the high sensitivity of the method we will soon also see more time dependent studies which will allow to monitor changes within ultrathin organic layers in real time.

References

1. J. Stöhr, *NEXAFS Spectroscopy*, (Springer, Berlin Heidelberg, 1992), pp. 1–403
2. J. L. Solomon, R. J. Madix, J. Stöhr, Surf. Sci. **255**, 12 (1991)
3. J. Kattner, H. Hoffmann, in *Handbook of Vibrational Spectroscopy*, ed. by J. M. Chalmers, P. R. Griffiths (John Wiley & Sons Ltd, Chichester, 2002), p. 1009
4. J. Heidberg, E. Kampshoff, R. Kühnemuth, O. Schönekäs, M. Suhren, J. Electron Spectrosc. Relat. Phenom. **54/55**, 945 (1990)
5. Y. Wang, A. Glenz, M. Muhler, Ch. Wöll, Rev. Sci. Instr. **80,** 113108 (2009)
6. B. E. Hayden, in *Vibrational Spectroscopy of Molecules on Surfaces*, ed. J. T. Yates, T. E. Madley, (John Wiley & Sons Ltd, New York, 1987), p. 267
7. P. S. Bagus, K. Weiss, A. Schertel, Ch. Wöll, W. Braun, C. Hellwig, C. Jung, Chem. Phys. Lett. **248**, 129 (1996)
8. D. Hübner, F. Holch, M. L. M. Rocco, K. C. Prince, S. Stranges, A. Schöll, E. Umbach, R. Fink, Chem. Phys. Lett. **415**, 188 (2005)
9. K. Weiss, P. S. Bagus, Ch. Wöll, J. Chem. Phys. **111**, 6834 (1999)
10. S. G. Urquhart, R. Gillies, J. Phys. Chem. A **109**, 2151 (2005)
11. D. Fuhrmann, D. Wacker, K. Weiss, K. Hermann, M. Witko, Ch. Wöll, J. Chem. Phys. **108**, 2651 (1998)

12. K. Hermann, L. G. M. Pettersson, M.E. Casida, C. Daul, A. Goursot, A. Koester, E. Proynov, A. St-Amant, D. R. Salahub, contributed authors: V. Carravetta, H. Duarte, C. Friedrich, N. Godbout, J. Guan, C. Jamorski, M. Lebuf, M. Leetmaa, M. Nyberg, S. Patchkovskii, L. Pedocchi, F. Sim, L. Triguero, A. Vela, StoBe-deMon version 3.1. http://www.fhi-berlin.mpg.de/KHsoftware/StoBe/index.html. Cited 12 Jul 2011
13. D. R. Salahub, M. E. Castro, R. Fournier, P. Calaminici, N. Godbout, A. Goursot, C. Jamorski, H. Kobayashi, A. Martinez, I. Papai, E. Proynov, N. Russo, S. Sirois, J. Ushio, A. Vela, in *Theoretical and Computational Approaches to Interface Phenomena*, ed. by H. Sellers, J. T. Gotlab (Plenum Press, New York, 1995), p. 187
14. D. R. Salahub, M. E. Castro, E. I. Proynov, in *Relativistic and electron correlation effects in molecules and solids N*, ed. by G. L. Malli, NATO ASI Series (Physics), vol. B318 (Plenum Press, New York, 1994), p. 411
15. W. Kohn, L. Sham, J. Phys. Rev. **140**, A1133 (1965)
16. H. Winick, in *Synchrotron Radiation Research*, ed. by H. Winick, S. Doniach (Plenum Press, New York, 1980)
17. G. Ertl, J. Küppers, *Low Energy Electrons and Surface Chemistry*, (VCH, Weinheim, 1985)
18. J. L. Wiza, Nucl. Instr. Methods **162**, 587 (1979)
19. PREVAC company, http://www.prevac.eu. Cited 13 Jul 2011
20. J. Stöhr, K. Baberschke, R. Jaeger, R. Treichler, S. Brennan, Phys. Rev. Lett. **47**, 381 (1981)
21. G. Hähner, Chem. Soc. Rev. **35**, 1244 (2006)
22. A. K. Ghosh, A. K. Naskar, S. Sengupta, L. Bizbiz, J. Labat-Robert, A. Alperovitch, L. Robert, The EVA-group, J. G. Chen, Surface Science Reports **30**, 1, (1997)
23. J. A. Horsley, J. Stöhr, A. P. Hitchcock, D. C. Newbury, A. L. Johnson, F. Sette, J. Chem. Phys. **83**, 6099 (1985)
24. B. E. Koel, J. E. Crowell, C. M. Mate, G. A. Somorjai, J. Phys. Chem. **90**, 2949 (1986)
25. H.-P. Steinrück, P. Heimann, W. Huber, P. Jakob, T. Pache, D. Menzel, J. Electron Spectrosc. Relat. Phenom. **52**, 91 (1990)
26. S. Aminpirooz, L. Becker, B. Hillert, J. Haase, Surf. Sci. **244**, L152 (1991)
27. K. Weiss, S. Gebert, M. Wühn, H. Wadepohl, Ch. Wöll, J. Vac. Sci. Technol. A **16**, 1017 (1998)
28. C. Mainka, P. S. Bagus, A. Schertel, T. Strunskus, M. Grunze, Ch. Wöll, Surf. Sci. **341**, L1055 (1995)
29. M. A. Van Hove, R. F. Lin, G. A. Somorjai, Phys. Rev. Lett. **51**, 778 (1983)
30. A. Wander, G. Held, R. Q. Hwang, G. S. Blackman, M. L. Xu, P. de Andres, M. A. Van Hove, G. A. Somorjai, Surf. Sci. **249**, 21 (1991)
31. J. B. Torrance, Acc. Chem. Res. **12**, 79 (1979)
32. T.-Ch. Tseng, Ch. Urban, Y. Wang, R. Otero, S. L. Tait, M. Alcamí, D. Écija, M. Trelka, J. M. Gallego, N. Lin, M. Konuma, U. Starke, A. Nefedov, A. Langner, Ch. Wöll, M. Á. Herranz, F. Martín, N. Martín, K. Kern, R. Miranda, Nat. Chem. **2**, 374, (2010)
33. R. G. Nuzzo, D. L. Allara, J. Amer. Chem. Soc. **105**, 4481 (1983)
34. J. C. Love, L. A. Estroff, J. K. Kriebel, R. G. Nuzzo, G. M. Whitesides, Chem. Rev. **105**, 1103 (2005)

35. A. Ulman, *Self-Assembled Monolayers of Thiols (Thin Films)*, (Elsevier Science and Technology 1998)
36. F. Schreiber, Prog. Surf. Sci. **65**, 151 (2000)
37. M. Kind, Ch. Wöll, Progr. Surf. Sci. **84**, 230 (2009)
38. O. Shekhah, H. Wang, M. Paradinas, C. Ocal, B. Schüpbach, A. Terfort, D. Zacher, R. A. Fischer, Ch. Wöll, Nat. Mater. **8**, 481 (2009)
39. O. Shekhah, H. Wang, T. Strunskus, P. Cyganik, D. Zacher, R. Fischer, Ch. Wöll, Langmuir **23**, 7440 (2007)
40. O. Shekhah, H. Wang, D. Zacher, R. A. Fischer, Ch. Wöll, Angew. Chem. Int. Ed. **48**, 5038 (2009)
41. S. Yoshimoto, Bull. Chem. Soc. Jpn. **7**9, 1167 (2006)
42. C. Silien, M. Buck, G. Goretzki, D. Lahaye, N. R. Champness, T. Weidner, M. Zharnikov, Langmuir **25**, 959 (2009)
43. Y. Zubavichus, M. Zharnikov, Y. J. Yang, O. Fuchs, E. Umbach, C. Heske, A. Ulman, M. Grunze, Langmuir **20**, 11022 (2004)
44. J.Liu, B. Schüpbach, A. Bashir, O. Shekhah, A. Nefedov, M. Kind, A. Terfort, Ch. Wöll, Phys. Chem. Chem. Phys. **12**, 4459 (2010).
45. S. Hövel, C. Kolczewski, M. Wühn, J. Albers, K. Weiss, V. Staemmler, Ch. Wöll, J. Chem. Phys. **112**, 3909 (2000)
46. C. Kolczewski, R. Puttner, O. Plashkevych, H. Agren, V. Staemmler, M. Martins, G. Snell, A. S. Schlachter, M. Sant'Anna, G. Kaindl, L. G. M. Pettersson, J. Chem. Phys. **115**, 6426 (2001)
47. J. L. Baudour, Acta Crystallogr. Sect. B: Struct. Sci. **47**, 935 (1991)
48. J. L. Baudour, H. Cailleau, W. B. Yelon, Acta Crystallogr., Sect. B: Struct. Crystallogr. Cryst. Chem. **33**, 1773 (1977)
49. A. Almenningen, O. Bastiansen, L. Fernholt, B. N. Cyvin, S. J. Cyvin, S. Samdal, J. Mol. Struct. **128**, 59 (1985)
50. M. J. Frisch, GAUSSIAN 03 (Revision E.01), Gaussian, Inc., Wallingford, CT, 2004.
51. S. Stepanow, T. Strunskus, M. Lingenfelder, A. Dmitriev, H. Spillmann, N. Lin, J. V. Barth, Ch. Wöll, K. Kern, J. Phys. Chem. B **108**, 19392 (2004)
52. S. Stepanow, M. Lingenfelder, A. Dmitriev, H. Spillmann, E. Delvigne, N. Lin, X. Deng, C. Cai, J. V. Barth, K. Kern, Nature Materials **3**, 229 (2004)
53. J. V. Barth, G. Costantini, K. Kern, Nature **437**, 671 (2005)
54. M. E. Cañas-Ventura, F. Klappenberger, S. Clair, S. Pons, K. Kern, H. Brune, T. Strunskus, Ch. Wöll, R. Fasel, J. V. Barth, J. Chem. Phys. **125**, 184710 (2006)
55. A. Tekiel, J. S. Prauzner-Bechcicki, S. Godlewski, J. Budzioch, M. Szymonski, J. Phys. Chem. C **112**, 12606 (2008)
56. M. Watkins, T. Trevethan, M. L. Sushko, A. L. Shluger, J. Phys. Chem. C **112**, 4226 (2008)
57. P. Rahe, M. Nimmrich, A. Nefedov, M. Naboka, Ch. Wöll, A. Kühnle, J. Phys. Chem. C **113**, 17471 (2009)
58. S. Reiss, H. Krumm, A. Niklewski, V. Staemmler, Ch. Wöll, J. Chem. Phys. **116**, 7704 (2002)
59. A. P. Hitchcock, C. Morin, X. Zhang, T. Araki, J. Dynes, H. Stöver, J. Brash, J. R. Lawrence, G. G. Leppard, J. Electron Spectrosc. Relat. Phenom. **144-147**, 259 (2005)

Index